Front. Eng. Manag. 2019, 6(2): 207–220
https://doi.org/10.1007/s42524-019-0016-5

RESEARCH ARTICLE

Ying ZHOU, Wan WANG, Hanbin LUO, Yan ZHANG

Virtual pre-assembly for large steel structures based on BIM, PLP algorithm, and 3D measurement

Abstract The current physical pre-assembly method of large steel structures is time consuming and costly and requires large sites. Thus, the pre-assembly of large steel structures in a virtual way, starting from building information modeling (BIM), is an interesting alternative to the physical one. In this study, an innovative method for virtual pre-assembly is proposed on the basis of BIM, plane-line-point algorithm, and 3D measurement. This method determines the optimal analytical least squares of the various built components. The technique verifies the feasibility of the steel structure assembly and the fulfillment of the design geometries, starting from the real data obtained by an accurate metric survey of the fabricated steel elements. The method is applied to a real case, and obtained results largely satisfy the prefixed research objectives. Suggestions to improve the proposed method are also discussed.

Keywords steel structure, pre-assembly, BIM, plane-line-point, 3D measurement

1 Introduction

Large steel structures have been used widely in the construction field since the 1980s due to their high strength, stiffness, adequate deformation capacity, and stress redistribution ability (Bjorhovde, 2012). Large steel structure elements are usually pre-assembled at the factory and then transported to the site for hoisting and welding to accelerate construction progress (Case et al., 2014). The shape and size of steel structures after molding seriously affect the success or failure of subsequent assembling work (Spence et al., 1993). Therefore, the steel components must be pre-assembled at the factory to check whether the components can be assembled to ensure successful assembly of these components in the construction site (Li et al., 2016).

Detecting the steel structures is important not only before but also during pre-assembly. The traditional detection methods include steel ruler examination, pulling wire, and lofting plumb line, which are used to detect whether the steel structures satisfy the design requirements. The detection process is complicated and time consuming. The traditional pre-assembly of large steel structures is laborious and requires lifting equipment and large sites (Ding et al., 2012). Some factories cannot provide large-scale assembly sites, thereby making pre-assembly work impossible; other factories can provide pre-assembly sites, but a large number of assembly jigs need to be set before the pre-assembly of steel components; this process is laborious and time consuming, requires large material resources, and harms the environment (Chen et al., 2015). The process also requires high rigidity and load-bearing capacity of the assembly jigs, thereby complicating the pre-assembly work of steel components (Liu et al., 2007).

Scholars have conducted considerable research and proposed a digital simulated pre-assembly method to reduce cost, reach high precision, shorten construction duration, and avoid requirement of large sites of the pre-assembly of large-scale steel structures. Tamai et al. (2002) proposed the computerized assembly test system (CATS) and used the system to a steel bridge in Japan. A method of digital simulated pre-assembly was used in the annular banded steel truss of the Shanghai Center Building by Ding et al. (2012). The application of computer-simulated pre-assembly method combined with the ATLAS $(1 + 1)\times 600$ MW supercritical coal-fired power station in Turkey was also described by Lan et al. (2013). Wang et al. (2016) used the similar digital simulation assembly method to Wuhan Nijiang Lake Bridge.

These previous works reveal that the current digital simulation pre-assembly technology is still in its infancy,

Received May 9, 2018; accepted December 16, 2018

Ying ZHOU, Wan WANG (✉), Hanbin LUO, Yan ZHANG
School of Civil Engineering and Mechanics, Huazhong University of Science and Technology, Wuhan 430074, China
E-mail: wangwan@hust.edu.cn

and the ideas are nearly the same. Specifically, a 3D designed model of the structure components is established first. Then, all surfaces of the physical components are measured with a total station, a camera, or a 3D scanner to build the fabricated model of the physical components. Finally, the fabricated model of the components is compared with the designed model, corrected, and simulated for pre-assembly. Coordinate alignment is the precondition for the comparison of two models and related to the precision of the entire virtual pre-assembly process. However, previous pre-assembly studies have failed to elaborate the method of coordinate alignment. Checking whether the pre-assembly error of the model satisfies the deviation requirement is the key to digital simulation pre-assembly. The predecessors have also conducted many different attempts to analyze this topic, but the ideas are the same and all need to manually compare whether the assembly data of the interface meet the allowable deviation requirement. The deviation should be less than 2.0 mm for steel beam, which is based on the national standard "Code for Acceptance of Construction Quality of Steel Structures" in China. The benefits of the above-mentioned digital simulation pre-assembly technology have been rationalized, but the algorithm of coordinate alignment still needs to be studied deeply because the precision of the subsequent processes, such as inspecting errors and virtual pre-assembly, is difficult to achieve (Meng, 2017). This technology also requires new methods to reduce the time of measuring the physical components and inspecting errors manually because the number of feature points of a large steel structure is large.

In the proposed virtual pre-assembly method of alignment, comparison and calibration (ACC) in this study, the measurement work was performed synchronously with the reconstruction of the real-time model of physical components to avoid data conversion and huge workload. Intuitive assembly graphics were provided to observe the effect of the assembly easily. Plane-line-point (PLP) algorithm was used to align coordinates. The maximum of the deviation of the measuring tool was 0.43 mm, which is considerably lesser than the allowable deviation requirement (2 mm). The entire assembly process was completed in the same software system, thereby providing a convenient method for virtual assembly of large steel structures.

2 Literature review

Building information modeling (BIM) has attracted considerable attention in the construction industry (Azhar et al., 2008a; Azhar et al., 2008b; Lu and Korman, 2010). This technology is defined as a digital representation of physical and functional characteristics of a facility (Smith, 2007). BIM, which contains all the up-to-date information related to the facility, is a great tool used by all parts involved in the construction to make management decisions during the entire lifecycle of the facility, from the earliest conception to the demolition. A BIM can be used for many purposes: renderings, various design analyses, fabrication drawings, construction sequencing, interference and collision detection, lifecycle cost analysis, storage of the geometrical features of the as-built structure, and checking of its assemblability.

The method of fabricated model rebuilding forms an integral part of the virtual pre-assembly process. Researchers have proposed various methods to transform the physical object into a fabricated model in the pre-assembly system. Barone et al. (2012) proposed a method combining an optical scanner and a stereo vision system, in which the optical scanner was used for block measurement and the stereo vision system was utilized to remotely track a 3D scanner and perform panoramic stitching. Paoli and Razionale (2012) proposed a measurement method based on optical scanners and mechanical tracking, which used a scanner to measure large objects in blocks and then performed panoramic stitching through mechanical tracking coordinates. The basic idea of the methods above is to measure the large object multiple times and then splice the 3D point cloud. However, the methods above cannot be used to measure large steel plates because they have a curvature that changes inconsiderably and a texture that is unstable and insufficient.

In Japan, CATS was proposed by Tamai et al. (2002). The shop assembly system used a charge coupled device camera to photograph each member of the completed bridge. The member shapes were input into a computer as 3D data, and a simulated shop assembly was executed in the computer after confirming the member shapes. Measurement of the member with a length of 15 m took 50 min, and arrangement of the measuring equipment was difficult. Moreover, data should be input into a computer in the 3D CAD model conversion. Li et al. (2016) used the TRITOP system to measure the feature points of components and then assembled them with the general algorithm. The method regarded coding points as the main body. However, the number of coding points was limited, and some locations were inconvenient to place the coding points and encode. The thickness of the point would also affect the measurement. The assembly process was mainly based on the rods, and the outer contour was not checked.

Lan et al. (2013) used a total station to measure the feature points of steel structures. Then, the coordinate was transformed in CAD to form feature model through the feature points. Finally, whether these points could be assembled was determined through the connection relationship. Tang et al. (2009) hoisted the components onto the assembly jigs first and then used the total station to detect the control points. The control points were compared to evaluate whether they could be assembled. The parts of the non-control points were not measured, and they still need to be hoisted and then compared. Case et al.

(2014) first classified the components according to the geometric shape of the structural components and then measured the center position of the joint holes of each node and pipe with the total station. Thereafter, the coordinates of measurement points, associated with the design coordinates, were stored into the matrix of $n\times3$. Topological relation analysis was used for alignment and the general analysis method for assembly. Measuring the coordinates of a component with a total station is a traditional measuring method because the fabricated model cannot be obtained directly from the measured coordinate data. The fabricated model cannot be constructed only by measuring the boundary points. Thus, a large number of feature points, including the points on the plane, must be measured. Measuring a large number of points of data increases not only the measurement workload but also the workload of the subsequent process of rebuilding fabricated model. Notably, accidental errors will be produced during the process of rebuilding fabricated model from the coordinate data.

Coordinate alignment is necessary for the virtual pre-assembly process. However, previous virtual pre-assembly works have failed to describe the algorithm of coordinate alignment. In the aircraft industry, scholars have conducted considerable research on the coordinate alignment and proposed three algorithms of alignment based on the shape feature of the objects: three-point, one-plane and two-point, and PLP algorithms. Li et al. (2017) aligned the coordinates of two models by positioning the three points of the scanned object that were not on the same straight line. However, the three-point feature generally needs to be obtained indirectly through other geometric features, such as the center of the feature, cone, cylinder, and ridge intersection. The extraction requirement of the three-point alignment midpoint is realized through the construction command. Chen et al. (2013) selected two cylindrical positioning points and one web plate on the components. First, the newly created reference information was redefined by the spatial coordinate position. Then, the corresponding reference coordinate information of the CAD model was added to the created reference information in the command box. Finally, the two-point coordinate alignment command was used in the system to complete the coordinate alignment. Leão et al. (2017) chose a bottom plate, a sideline on one web plate, and a point on the top plate of the girder. The subsequent processes were the same as the method of Chen et al. (2013). However, the one-plane and two-point alignment algorithm is usually used for objects with more than one evident bulge or depression. During the measuring process, the relative position of fabricated model and BIM will change when the dynamic mode is not chosen. For the virtual pre-assembly method proposed in this study, the curvature of the large steel box girders changes inconsiderably and the plates are smooth and thus have no evident feature points. Therefore, three-point or one-plane and two-point algorithm cannot be used. Meanwhile, the PLP algorithm does not require feature points. The PLP algorithm can fix the entire six degrees of freedom of the fabricated models by choosing a plane, a line, and a point on the components. Thus, they cannot move or rotate even when the physical components are moved. The PLP algorithm can keep the relative position of fabricated model and BIM stationary. Therefore, the errors of coordinate alignment can be decreased to reduce the accumulative errors of the entire virtual pre-assembly. In other words, the precision of the entire virtual pre-assembly will be improved.

3 Methodology

The proposed virtual pre-assembly method of ACC for steel structures in this study can solve the separation problem of measurement and virtual assembly of structures. The entire pre-assembly process is completed in the same software system, thereby providing a convenient method for offline pre-assembly of large steel structures. The method is divided into two main parts: one is the measurement and inspection process, and the other is the virtual assembly process. The measurement and detection process has two important steps. On the one hand, the coordinates of the component to be measured and those of the BIM should be aligned before the formal measurement work begins. On the other hand, the actual model and BIM should be counted after the component is measured. The virtual assembly works as follows. First, the BIM is modified before the formal virtual assembly to obtain the real-time model of the physical components. Then, 3D and 2D comparisons of the virtual assembly process are conducted. The BIM should be established on the basis of the design values of the components. When using light pens to measure components, the light pen should be kept perpendicular to the plane where the measurement points are located to achieve the best measurement effect. For easy understanding, the entire method is represented in a flowchart (Fig. 1).

3.1 Alignment by PLP algorithm

The BIM is constructed on the basis of the design values of the components in the Revit software. The BIM is parameterized for follow-up model revisions (Liu et al., 2016).

After importing the BIM into the system, the measurement object must be aligned with the coordinate system of the BIM, which is the basis for subsequent measurement work (Sun and Yao, 2008). For large steel structures, such as those with large reference surface, the PLP algorithm can be used for alignment. The PLP alignment algorithm is an accurate alignment method because it limits the components from all six degrees of freedom (Radowick, 2003). The method establishes the relationship between the

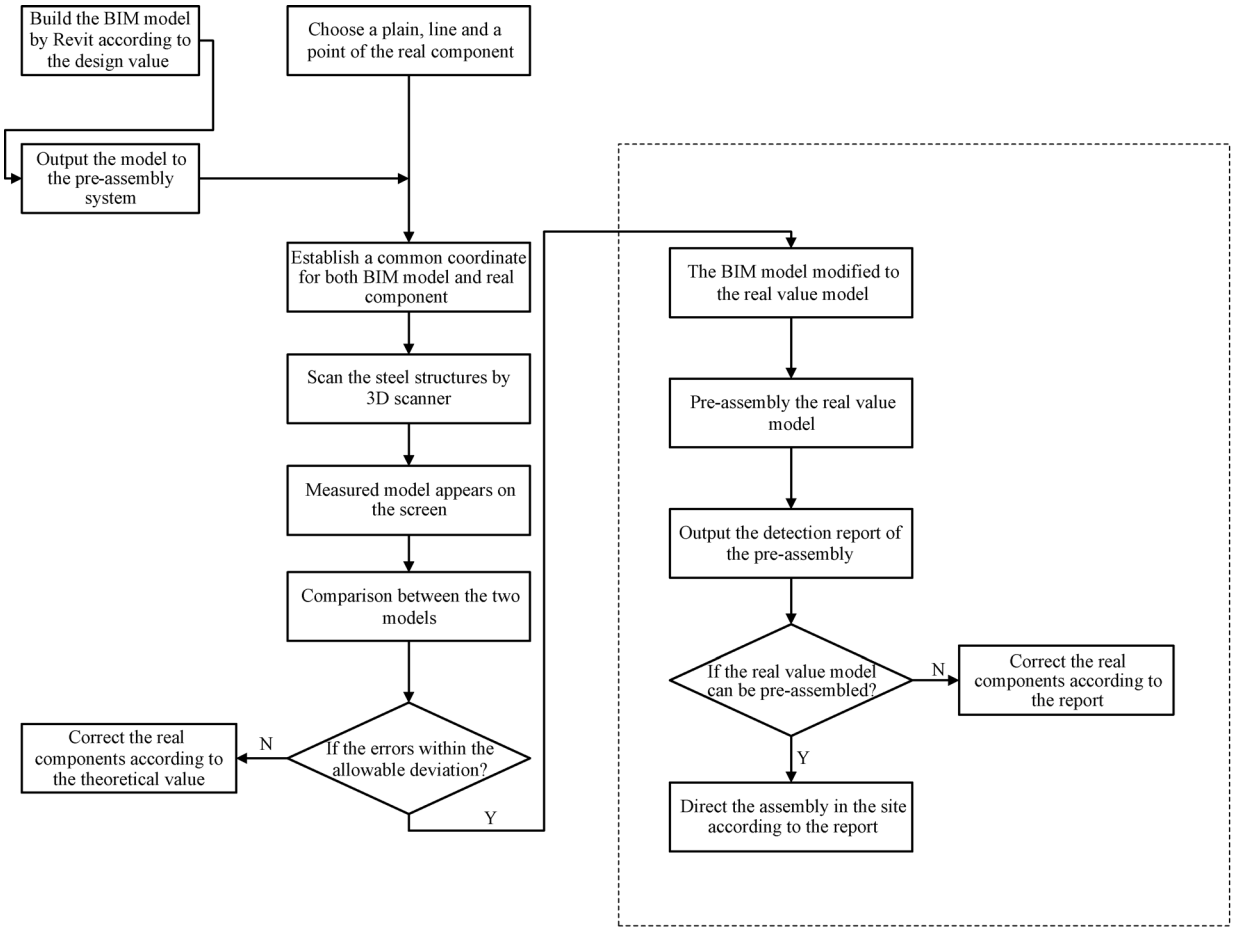

Fig. 1 Flowchart for the ACC pre-assembly method

real components and the coordinates of the BIM by measuring the values of a plane, a line, and a point on the component.

The PLP algorithm is used to set the same coordination as the BIM model for the real-time model which is going to be measured. Figure 2 shows the object and the BIM model of the object. The bottom surface S of the BIM model is chosen in the system. The plane S' of the object is chosen by the light pen in the actual environment, and then will be displayed in the system. Values of the plane S are assigned to the plane S' to keep the real-time model of the object and the BIM model on the same plane in the system. Therefore, the real-time model will not pitch, roll or translate up-down. In other words, the degrees of freedom of the real-time model are reduced to three. Then the real-time model can just yaw and translate left-right and forward-back. Similarly, the line L of the BIM model and L' of the object are both chosen. Now the real-time model will not translate forward-back or left-right either. The degrees of freedom of the real-time model are reduced to only one. Finally, the position of the real-time model will

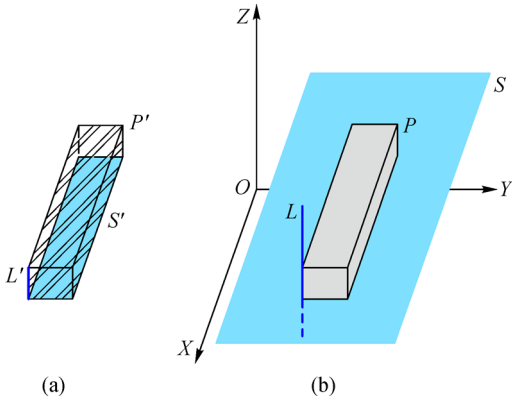

Fig. 2 PLP algorithm works between (a) object and (b) BIM model

be fixed by fixing one point. Thus, the vertexes P and P' are chosen for they are easy to find.

PLP alignment is accurate. However, if the effective combination of alignment is not satisfied, then PLP alignment will not work. The combination of plane, line

and point above is just one situation. Table 1 lists the effective combination of the PLP algorithm.

Table 1 Efficient combination of coordination alignment of PLP algorithm

Plane	Line	Point
YOZ	*X* or *Y*	Any point
XOZ	*Y* or *Z*	Any point
XOY	*Z* or *X*	Any point

Note: (1) The plane, the line and the point above in every efficient combination are on the object and designed/BIM model correspondingly as shown in Fig. 2; (2) the chosen line should be normal to the chosen plane; (3) the point should be on the object and designed/BIM model but not be either on the chosen plane or the chosen line.

Alignment of the coordinate system of the fabricated model and the BIM can be achieved by the rotation matrix $\boldsymbol{R}$ and the translation matrix $\boldsymbol{T}$ (MacWilliams et al., 1998). The 3D rotation can make the coordinate systems of the fabricated model and the BIM reach a spatially parallel state; then, the two-coordinate system can be translated once to completely overlap (Hara et al., 2009).

The derivation of the rotation matrix $\boldsymbol{R}$ can be set to rotate γ around the Z axis, rotate β around the Y axis, and rotate α around the X axis. Specifically, the rotation sequence is XYZ, and the rotation matrix $\boldsymbol{R}$ is

$$\begin{aligned}\boldsymbol{R}(\alpha,\beta,\gamma) &= \boldsymbol{R}_x\cdot\boldsymbol{R}_y\cdot\boldsymbol{R}_z\\ &= \begin{bmatrix}1 & 0 & 0\\ 0 & s_x & -c_x\\ 0 & c_x & s_x\end{bmatrix}\cdot\begin{bmatrix}s_y & 0 & -c_y\\ 0 & 1 & 0\\ c_y & 0 & s_y\end{bmatrix}\cdot\begin{bmatrix}s_z & -c_z & 0\\ c_z & s_z & 0\\ 0 & 0 & 1\end{bmatrix}\\ &= \begin{bmatrix}s_ys_z & -s_yc_z & -c_y\\ -c_xc_ys_z+s_xc_z & c_xc_yc_z+s_xs_z & -c_xs_y\\ s_xc_ys_z+c_xc_z & -s_xc_yc_z+c_xs_z & s_xs_y\end{bmatrix},\end{aligned} \tag{1}$$

where

$$\begin{cases}c_x=\sin\alpha,\ s_x=\cos\alpha,\\ c_y=\sin\beta,\ s_y=\cos\beta,\\ c_z=\sin\gamma,\ s_z=\cos\gamma.\end{cases}$$

Counterclockwise is defined as positive direction of all angles. Correspondingly, the translational matrix $\boldsymbol{T}$ is used to translate (x,y,z) to (x',y',z'). The projection distance in three directions can be represented by t.

The point-to-point transformation can be obtained as follows:

$$\begin{cases}x'=x+t_x,\\ y'=y+t_y,\\ z'=z+t_z,\end{cases} \tag{2}$$

$$\begin{aligned}&\begin{pmatrix}x' & y' & z' & 1\end{pmatrix}\\ &=\begin{pmatrix}x & y & z & 1\end{pmatrix}\begin{bmatrix}1 & 0 & 0 & 0\\ 0 & 1 & 0 & 0\\ 0 & 0 & 1 & 0\\ t_x & t_y & t_z & 1\end{bmatrix}.\end{aligned} \tag{3}$$

From the rotation matrix, the translational matrix, and the common point, the second scanning point can be described as $\boldsymbol{Q}=\boldsymbol{R}\cdot\boldsymbol{P}+\boldsymbol{T}$.

$\boldsymbol{Q}=(x,y,z)$ and $\boldsymbol{P}=(x',y',z')$ are points in different coordinate systems. The mathematical expression above is mainly used for the spatial transformation between two point sets.

3.2 Comparison of designed and fabricated models

In this method, the measurement and detection process are the premise of the subsequent virtual assembly (Crispin and Rankov, 2007). In other words, this process is mainly for the subsequent simulation assembly work (Li et al., 2013). Therefore, when measuring components with a light pen meter, the control section or point is mainly measured.

Digital-to-analog comparisons are performed in a digital simulation assembly system to verify whether the real components are qualified (Fan et al., 2009). If the component is unqualified, then the value of the offset between the actual measured component and the design drawing is determined and used as input. The measured component is returned to the factory to correct the offset value of the connection. If the component is qualified, then the model is corrected. The digital-to-analog comparison process includes 3D and 2D comparisons. Specifically, 3D comparison is used to perform bias analysis on all data measured by a certain unit to obtain the deviation distribution, whereas 2D comparison is adopted to analyze the deviation of the characteristic section. Before 2D comparison is performed, the view needs to be pre-defined on the basis of different perspectives, such as left and right views.

After the light pen is used to measure the coordinates of a certain characteristic point, the system processor starts the digital-to-analog comparison. That is, the comparison work is nearly synchronous with the measurement work. After the measurement work is completed, the comparison result is generated. This real-time comparison avoids the operational stress caused by concentration comparisons on the processor.

3.3 Calibration of BIM

Virtual assembly emphasizes the virtual environment of the assembly environment, that is, the process of artificial assembly is simulated by the system program (Jayaram

et al., 1997). The real value model of the component should restore the geometric features of the control section or point of the component to the greatest degree to ensure convincing assembly result.

In this method, the light pen instrument is used to measure the feature cross section or point of the component rather than performing a full scan. Therefore, the real value model of the component does not directly form. After the digital-to-analog comparison, the processor needs to be modified on the BIM on the basis of such conditions for components that meet the design specifications. Accordingly, the BIM can restore the geometric features of the real components.

In practice, the assembling process of components only occurs at a certain section or even at a specific point.

As shown in Fig. 3, several points appear around a space line. In the measurement work with a light pen, a large number of points are measured around the shape of the component. Therefore, a method of space straight line and curve fitting is applied to the measurement point, and the measurement is conveniently and intuitively processed. For the straight line fitting of the measurement points, the least square method is usually used. However, the fitting effect can only maintain the best in one direction because selecting different independent and dependent variables will lead to different fitting straight lines. Here, the overall least square method is used for fitting to obtain an accurate fitting line and the best fitting effect (Han et al., 2017). This study assumes m observation points and considers that the coordinate value of the observation point and the coefficient matrix have errors. The expression of the linear equation for 2D space is

$$y_i = \hat{a}x_i + \hat{b},\ i = 1,2,...,m, \tag{4}$$

where $\hat{a}$ is the slope estimate value, $\hat{b}$ is the intercept estimate value, and (x_i,y_i) is the coordinate of the observation point. a and b are the approximate values of $\hat{a}$ and $\hat{b}$, respectively.

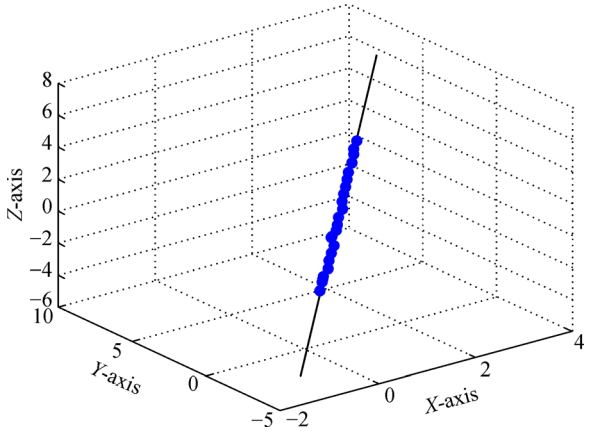

Fig. 3 Fitting of 3D line

$$\begin{cases} \hat{a} = a + \Delta a, \\ \hat{b} = b + \Delta b. \end{cases}$$

Considering that the observation point also has errors, the linear condition equation is

$$y_i + v_{yi} = \hat{a}(x_i + v_{x_i}) + \hat{b},\ i = 1,2,...,m, \tag{5}$$

where

$$v_{y_i} = [x_i \quad 1]\begin{bmatrix} \Delta a \\ \Delta b \end{bmatrix} + (ax_i + b - y_i).$$

The error equation can be described by the error-in-variable (EIV) model as

$$(\boldsymbol{A} + \boldsymbol{E}_A)\Delta X = \boldsymbol{l} + \boldsymbol{e}_l, \tag{6}$$

where

$$\boldsymbol{A} = \begin{bmatrix} x_1 & 1 \\ x_2 & 1 \\ \vdots & \vdots \\ x_m & 1 \end{bmatrix}, \boldsymbol{l} = \begin{bmatrix} ax_1 + b - y_1 \\ ax_2 + b - y_2 \\ \vdots \\ ax_m + b - y_m \end{bmatrix}, \boldsymbol{E}_A = \begin{bmatrix} v_{y_1} \\ v_{y_2} \\ \vdots \\ v_{y_m} \end{bmatrix},$$

$$\Delta X = \begin{bmatrix} \Delta a \\ \Delta b \end{bmatrix},$$

and $\boldsymbol{E}_A$ and $\boldsymbol{e}_l$ are error vectors of $\boldsymbol{A}$ and $\boldsymbol{l}$, respectively.

Equation (6) can be written as follows:

$$(\boldsymbol{B} + \boldsymbol{D})\boldsymbol{Z} = \boldsymbol{0}, \tag{7}$$

where

$$\boldsymbol{B} = [\boldsymbol{l}|\boldsymbol{A}],\ \boldsymbol{D} = [\boldsymbol{e}_l|\boldsymbol{E}_A],\ \boldsymbol{Z} = \begin{bmatrix} 1 \\ \cdots \\ \Delta X \end{bmatrix} = \begin{bmatrix} 1 \\ \Delta a \\ \Delta b \end{bmatrix}.$$

The best-fitting straight line is solved using the total least square method. In fact, solving a certain matrix minimizes the norm of the perturbation matrix. In particular, once the conditions are met, the best-fit straight line can be obtained.

The 3D linear equation,

$$\frac{x - x_0}{A} = \frac{y - y_0}{B} = \frac{z - z_0}{C}, \tag{8}$$

is a continuum equation and not a simple linear relationship. Thus, this equation can be converted into a Gauss-Markov model to solve the problem. When the matrix formed by the observed value and the function model have errors, the EIV is called. The EIV model is solved by the least square method alone and thus cannot contain errors. Other methods, such as overall least square method, mixed least square method, weighted global least square method,

robust overall minimum, and two-time solution, can also be used. Considering that the gross errors are discriminated and the data errors are prevented during discrimination, this study selects the iterative algorithm of the overall least square method, determines the conditions, and supplements the computer program to improve the precision and efficiency of data processing.

After the transformation, Eq. (8) has the form:

$$\begin{cases} x = \dfrac{A}{C}(z-z_0) + x_0 = az + b, \\ y = \dfrac{A}{B}(z-z_0) + y_0 = cz + d. \end{cases} \tag{9}$$

When multiple sets of observations are available, the overall least square model is

$$(\boldsymbol{A} + \boldsymbol{E}_A)\boldsymbol{X} = \boldsymbol{L} + \boldsymbol{V}_L, \tag{10}$$

where

$$\boldsymbol{L} = \begin{bmatrix} x_1 \\ y_1 \\ \vdots \\ x_m \\ y_m \end{bmatrix}, \boldsymbol{V}_L = \begin{bmatrix} V_{x_1} \\ V_{y_1} \\ \vdots \\ V_{x_m} \\ V_{y_m} \end{bmatrix}, \boldsymbol{A} = \begin{bmatrix} z_1 & 1 & 0 & 0 \\ 0 & 0 & z_1 & 1 \\ \vdots & \vdots & \vdots & \vdots \\ z_m & 1 & 0 & 0 \\ 0 & 0 & z_m & 1 \end{bmatrix},$$

$$\boldsymbol{E}_A = \begin{bmatrix} 0 & V_{z_1} & 0 & 0 \\ 0 & 0 & 0 & V_{z_1} \\ \vdots & \vdots & \vdots & \vdots \\ 0 & V_{z_m} & 0 & 0 \\ 0 & 0 & 0 & V_{z_m} \end{bmatrix}, \boldsymbol{X} = \begin{bmatrix} a \\ b \\ c \\ d \end{bmatrix}.$$

$\boldsymbol{L}$ is the coordinate matrix of the measurement value of x and y; $\boldsymbol{V}_L$ is the correction value of the measurement value of x and y; $\boldsymbol{A}$ is the coordinate matrix of the measurement value of z; $\boldsymbol{E}_A$ is the revise value of the z value, that is, the error revise of the coefficient matrix; and $\boldsymbol{X}$ is the unknown parameter, that is, the coefficient matrix. Mathematical expression Eq. (10) is written in the form:

$$\boldsymbol{L} = (\boldsymbol{A} + \boldsymbol{E}_A)\boldsymbol{X} - \boldsymbol{V}_L. \tag{11}$$

Evidently, the matrixes in Eq. (11) are linear. The least square method $\Phi = \boldsymbol{V}^{\mathrm{T}}\boldsymbol{P}\boldsymbol{V} = \min$ indicates that, if $\boldsymbol{P}$ is a non-diagonal matrix, then the observed values are correlated. Otherwise, the observed values are uncorrelated. The equation can be solved by

$$\Phi = \boldsymbol{V}^{\mathrm{T}}\boldsymbol{P}\boldsymbol{V} = p_1 v_1^2 + p_2 v_2^2 + \cdots + p_n v_n^2 = \min. \tag{12}$$

The problem can also be solved by

$$\sum_{i=1}^{n} \left(\hat{L}_i - L_i\right)^2 + \sum_{i=1,j=1}^{i=n,j=t} \left(\hat{A}_{ij} - A_{ij}\right)^2 = \min. \tag{13}$$

Therefore, the problem is transformed to obtain an optimal solution of least square method. This problem has been investigated by School of Geodesy and Geomatics in Wuhan University. $\boldsymbol{L}$ is introduced into Eqs. (2)–(17) for simplification.

$$\left(\sum_{i=1}^{n}\sum_{j=1}^{t} \hat{A}_{ij}\hat{X}_j - L_i\right)^2 + \sum_{i=1}^{n}\sum_{j=1}^{t} \left(\hat{A}_{ij} - A_{ij}\right)^2 = \min$$

$$\Rightarrow \left(\sum_{i=1}^{n}\sum_{j=1}^{t} \hat{A}_{ij}\hat{X}_j\right)^2 - 2\sum_{i=1}^{n}\sum_{j=1}^{t} \hat{A}_{ij}\hat{X}_j L_i$$

$$+ \left(\sum_{i=1}^{n} L_i\right)^2 + \sum_{i=1}^{n}\sum_{j=1}^{t} \left(\hat{A}_{ij} - A_{ij}\right)^2 = \min. \tag{14}$$

The left mathematical expression is defined equal to F. Then, derivation calculus to $\boldsymbol{A}$, $\boldsymbol{X}$ is developed as follows:

$$\begin{cases} \dfrac{\partial F}{\hat{A_{11}}} = \left(\hat{A_{11}} - A_{11}\right) + \left(\sum\limits_{j=1}^{t} \hat{A_{1j}}\hat{X_j} - L_1\right)\hat{X_1} = 0, \\ \dfrac{\partial F}{\hat{A_{12}}} = \left(\hat{A_{12}} - A_{12}\right) + \left(\sum\limits_{j=1}^{t} \hat{A_{1j}}\hat{X_j} - L_1\right)\hat{X_2} = 0, \\ \vdots \\ \dfrac{\partial F}{\hat{A_{1t}}} = \left(\hat{A_{1t}} - A_{1t}\right) + \left(\sum\limits_{j=1}^{t} \hat{A_{1j}}\hat{X_j} - L_1\right)\hat{X_t} = 0, \\ \dfrac{\partial F}{\hat{A_{21}}} = \left(\hat{A_{21}} - A_{21}\right) + \left(\sum\limits_{j=1}^{t} \hat{A_{2j}}\hat{X_j} - L_2\right)\hat{X_1} = 0, \\ \vdots \\ \dfrac{\partial F}{\hat{A_{nt}}} = \left(\hat{A_{nt}} - A_{nt}\right) + \left(\sum\limits_{j=1}^{t} \hat{A_{nj}}\hat{X_j} - L_n\right)\hat{X_t} = 0, \\ \dfrac{\partial F}{\hat{X_1}} = \left(\sum\limits_{j=1}^{t} \hat{A_{1j}}\hat{X_j} - L_1\right)\hat{A_{11}} + \left(\sum\limits_{j=1}^{t} \hat{A_{2j}}\hat{X_j} - L_2\right)\hat{A_{21}} \\ \qquad + \cdots + \left(\sum\limits_{j=1}^{t} \hat{A_{nj}}\hat{X_j} - L_n\right)\hat{A_{n1}} = 0, \\ \vdots \\ \dfrac{\partial F}{\hat{X_t}} = \left(\sum\limits_{j=1}^{t} \hat{A_{1j}}\hat{X_j} - L_1\right)\hat{A_{1t}} + \left(\sum\limits_{j=1}^{t} \hat{A_{2j}}\hat{X_j} - L_2\right)\hat{A_{2t}} \\ \qquad + \cdots + \left(\sum\limits_{j=1}^{t} \hat{A_{nj}}\hat{X_j} - L_n\right)\hat{A_{nt}} = 0. \end{cases} \tag{15}$$

$n\times t$ equations are available for A_{ij}, and t equations are available for X_j. A_{ij} is an $n\times t$ matrix, and X_j is a t-order matrix. Thus, a unique solution of the equation exists. However, the 3D lines are different from the 2D ones because they are not simply linear. Accordingly, the equations above should be simplified further as follows:

$$\hat{A_{11}}-A_{11}+\left(\sum_{j=1}^{t}\hat{A_{1j}}\hat{X_j}-L_1\right)\hat{X_1}=0$$

$$\Rightarrow \hat{A_{11}}-A_{11}+\hat{X_1}\left(\hat{A_{11}}\hat{X_1}+\hat{A_{12}}\hat{X_2}+\cdots+\hat{A_{1t}}\hat{X_t}\right)-L_1\hat{X_1}=0$$

$$\Rightarrow \hat{A_{11}}+\hat{A_{11}}\hat{X_1^2}+\hat{A_{12}}\hat{X_2}\hat{X_1}+\cdots+\hat{A_{1t}}\hat{X_t}\hat{X_1}=A_{11}+L_1\hat{X_1}. \tag{16}$$

Using the same simplification methods above, all equations of the derivation calculus to $\boldsymbol{A}$ can be simplified as follows:

$$\begin{cases}(1+\hat{X_1^2})\hat{A_{11}}+\hat{X_1}\hat{X_2}\hat{A_{12}}+\cdots+\hat{X_1}\hat{X_t}\hat{A_{1t}}=A_{11}+L_1\hat{X_1},\\ \hat{X_1}\hat{X_2}\hat{A_{11}}+(1+\hat{X_2^2})\hat{A_{12}}+\cdots+\hat{X_2}\hat{X_t}\hat{A_{1t}}=A_{12}+L_1\hat{X_2},\\ \vdots\\ \hat{X_1}\hat{X_t}\hat{A_{11}}+\hat{X_2}\hat{X_t}\hat{A_{1t}}+\cdots+(1+\hat{X_t^2})\hat{A_{1t}}=A_{1t}+L_1\hat{X_t},\\ (1+\hat{X_2^2})\hat{A_{21}}+\hat{X_1}\hat{X_2}\hat{A_{22}}+\cdots+\hat{X_1}\hat{X_t}\hat{A_{2t}}=A_{21}+L_2\hat{X_1},\\ \vdots\\ \hat{X_1}\hat{X_t}\hat{A_{n1}}+\hat{X_2}\hat{X_t}\hat{A_{nt}}+\cdots+(1+\hat{X_t^2})\hat{A_{nt}}=A_{nt}+L_n\hat{X_t}.\end{cases} \tag{17}$$

All equations above can also be simplified in the form of matrix as follows:

$$\boldsymbol{N}_b\hat{\boldsymbol{A}}^{\mathrm{T}}=\boldsymbol{A}^{\mathrm{T}}+\hat{\boldsymbol{X}}\boldsymbol{L}^{\mathrm{T}}, \tag{18}$$

where $\boldsymbol{N}_b=\boldsymbol{E}+\hat{\boldsymbol{X}}\hat{\boldsymbol{X}}^{\mathrm{T}}$. Then, all equations of the derivation calculus to $\boldsymbol{X}$ can be simplified as follows:

$$\left(\sum_{j=1}^{t}\hat{A_{1j}}\hat{X_j}-L_1\right)\hat{A_{11}}+\left(\sum_{j=1}^{t}\hat{A_{2j}}\hat{X_j}-L_2\right)\hat{A_{21}}+\cdots$$

$$+\left(\sum_{j=1}^{t}\hat{A_{nj}}\hat{X_j}-L_n\right)\hat{A_{n1}}=0$$

$$\Rightarrow \hat{A_{11}^2}\hat{X_1}+\hat{A_{11}}\hat{A_{12}}\hat{X_2}+\cdots+\hat{A_{11}}\hat{A_{1t}}\hat{X_t}-L_1\hat{A_{11}}+\hat{A_{21}^2}\hat{X_1}$$

$$+\hat{A_{21}}\hat{A_{22}}\hat{X_2}+\cdots+\hat{A_{21}}\hat{A_{2t}}\hat{X_t}-L_1\hat{A_{21}}+\cdots+\hat{A_{n1}^2}\hat{X_1}$$

$$+\hat{A_{n1}}\hat{A_{n2}}\hat{X_2}+\cdots+\hat{A_{n1}}\hat{A_{nt}}\hat{X_t}-L_n\hat{A_{n1}}=0$$

$$\Rightarrow \sum_{i=1}^{n}\hat{A_{i1}^2}\hat{X_1}+\sum_{i=1}^{n}\hat{A_{i1}}\hat{A_{i2}}\hat{X_2}+\cdots+\sum_{i=1}^{n}\hat{A_{i1}}\hat{A_{it}}\hat{X_t}=\sum_{i=1}^{n}L_i\hat{A_{i1}}. \tag{19}$$

The remaining equations can be simplified as follows:

$$\begin{cases}\sum_{i=1}^{n}\hat{A_{i1}^2}\hat{X_1}+\sum_{i=1}^{n}\hat{A_{i1}}\hat{A_{i2}}\hat{X_2}+\cdots+\sum_{i=1}^{n}\hat{A_{i1}}\hat{A_{it}}\hat{X_t}=\sum_{i=1}^{n}L_i\hat{A_{i1}},\\ \sum_{i=1}^{n}\hat{A_{i1}}\hat{A_{i2}}\hat{X_1}+\sum_{i=1}^{n}\hat{A_{i2}^2}\hat{X_2}+\cdots+\sum_{i=1}^{n}\hat{A_{i2}}\hat{A_{it}}\hat{X_t}=\sum_{i=1}^{n}L_i\hat{A_{i2}},\\ \vdots\\ \sum_{i=1}^{n}\hat{A_{i1}}\hat{A_{it}}\hat{X_1}+\sum_{i=1}^{n}\hat{A_{i2}}\hat{A_{it}}\hat{X_2}+\cdots+\sum_{i=1}^{n}\hat{A_{it}^2}\hat{X_t}=\sum_{i=1}^{n}L_i\hat{A_{it}}.\end{cases} \tag{20}$$

All equations for $\boldsymbol{X}$ can be simplified in the form of matrix as follows:

$$\hat{\boldsymbol{A}}^{\mathrm{T}}\hat{\boldsymbol{A}}\hat{\boldsymbol{X}}=\hat{\boldsymbol{A}}^{\mathrm{T}}\boldsymbol{L}. \tag{21}$$

Therefore, the problem to find a unique solution from equations with many parameters is converted to solve the matrix equations below. Iterative methods can be used to solve the equations.

$$\begin{cases}\boldsymbol{N}_b\hat{\boldsymbol{A}}^{\mathrm{T}}=\boldsymbol{A}^{\mathrm{T}}+\hat{\boldsymbol{X}}\boldsymbol{L}^{\mathrm{T}},\\ \hat{\boldsymbol{A}}^{\mathrm{T}}\hat{\boldsymbol{A}}\hat{\boldsymbol{X}}=\hat{\boldsymbol{A}}^{\mathrm{T}}\boldsymbol{L}.\end{cases} \tag{22}$$

Iterative initial values can be obtained from the measured data.

4 Experiment

Figure 4 shows the virtual pre-assembly method of ACC, which was applied to a small steel box girder in the lab for the first time. Figure 5 shows the size of the girder. The designed model of the girder (DMG) (Fig. 6) was built in Revit in accordance with the design value. Thus, the two

Fig. 4 Steel box girder in lab

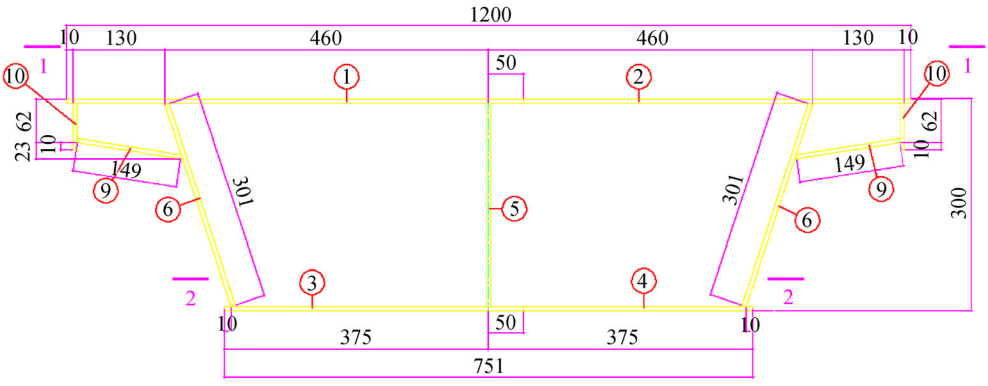

Fig. 5 Drawing of DMG: vertical (unit: mm)

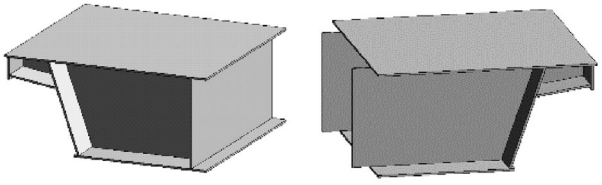

Fig. 6 Designed model of the girder

components of DMG were necessarily assembled. DMG was imported to the virtual pre-assembly system.

PLP method was used to build the coordination for the designed and fabricated models (Figs. 7 and 8). As the coordination was prepared, the measurement of the small steel girder started.

The fabricated model of the girder (FMG) appeared on the screen in real time while a laser was used to scan the boundary points of the steel box girder. The data comparison between FMG and DMG was accomplished in the system (Fig. 9), and the errors between FMG and DMG were given in real time. The entire pre-assembly work including modeling, building the coordination, scanning, data comparison, virtual pre-assembly, and generating report was accomplished at approximately 1.5 h. The scanning process took nearly 10 min. In this experiment, the errors were all within the allowable deviation. Thus, the two components of FMG could be assembled in the real environment. Thereafter, DMG could be modified by least square principle in the system to be similar to the real girder components. After the modification, DMG was converted to calibrated value model. Then the virtual pre-assembly work followed. Figure 10 displays the assembly results in the form of a chromatogram on the screen.

5 Case study

The investigated company is a steel structure manufacturing enterprise in China's central region. The steel structure via duct project in Wuhan is a key project of the company. In this bridge project, the steel box girder has a total length of 5355 m, 6 two-way lanes, a bridge width of 26–49 m, a steel consumption of 90218 t, and a construction period of 30 months. The dimensions of each steel box girder segment are 14.5 m long, 5.672 m wide, and 1.954 m high.

In the traditional assembly process, pre-assembly in the factory is required to ensure the steel box beam meets the on-site assembly requirements. The current study uses the above-mentioned virtual assembly method for the steel box girder section of the bridge project to verify the practicability.

Figure 11 shows the prefabricated site of the steel component factory, and Fig. 12 shows the cross section of the steel box girder used in the bridge project.

5.1 Virtual pre-assembly of steel box girder segments

The bridge project has 1826 segments. If traditional pre-assembly technology is used, then renting a large number of sites and manpower will be time consuming and costly. In this study, the above-mentioned virtual pre-assembly method was used to virtually pre-assemble the two components of the box girder segments. The BIM of the steel box girder components was built. The BIM should contain all the information of the steel structure components, that is, the material and other information should be included in addition to the dimensional design values. Figure 13 shows the BIM of the steel box girder component.

The BIM of the steel box beam components could be assembled within the allowable deviation. The BIM was introduced into the measurement system, and the coordinates of the steel box girder unit were aligned with those of the BIM. Then, the 3D scanning of the steel box girder was measured. The scan data were transmitted to the computer processor in real time, and the deviation value was displayed in real time.

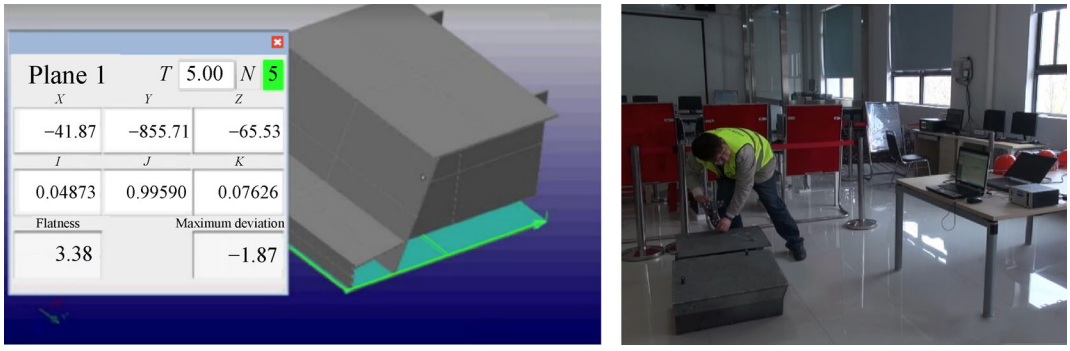

Fig. 7 Choosing a plane of real component

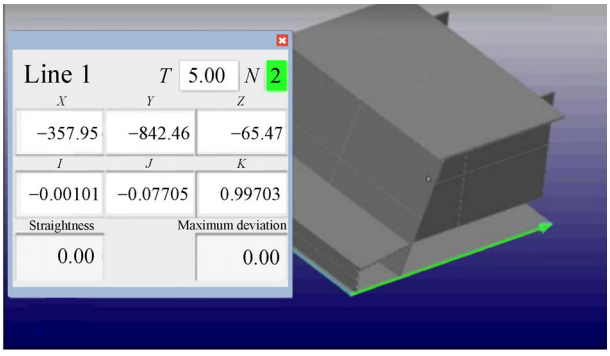

Fig. 8 Choosing a line of real component

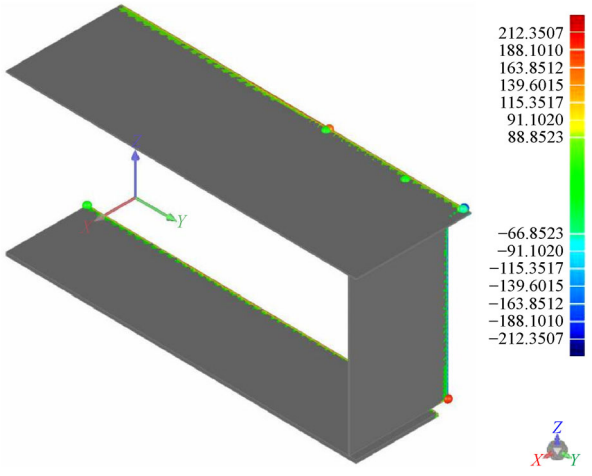

Fig. 9 Comparison between DMG and FMG

If the error in the size of the steel box girder unit model exceeds the allowable deviation, then a factory correction is required. The model sizes of the two steel box girder units measured this time were within the acceptable range. Thus, the model was modified to minimize the size of the real components. The correction process must still be performed in the measurement system. After the BIM was modified to a true value model, the pre-assembly process could be simulated in the system.

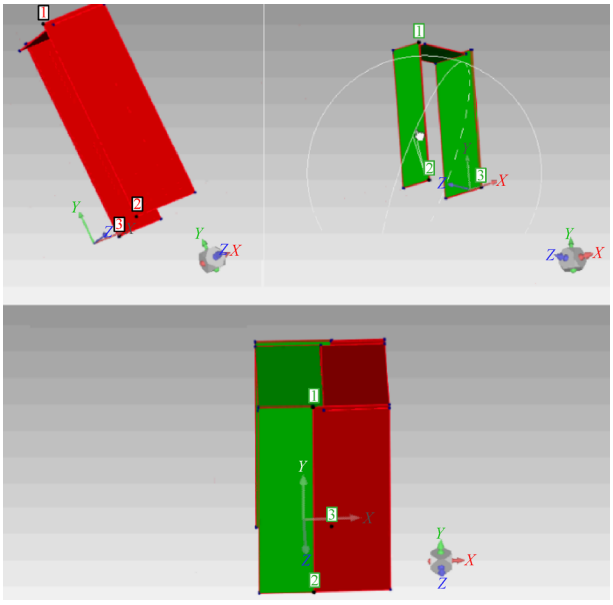

Fig. 10 Virtual pre-assembly

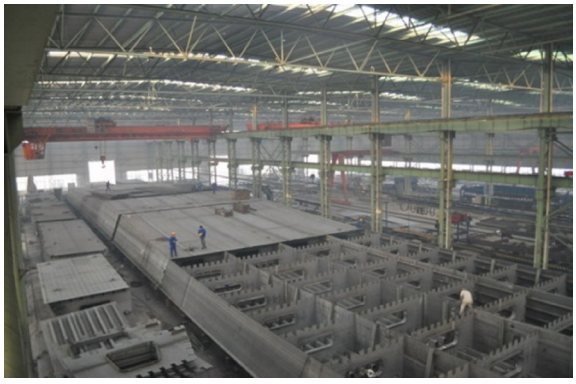

Fig. 11 Precast steel box girder in factory

Fig. 12 Cross sections of steel box girders

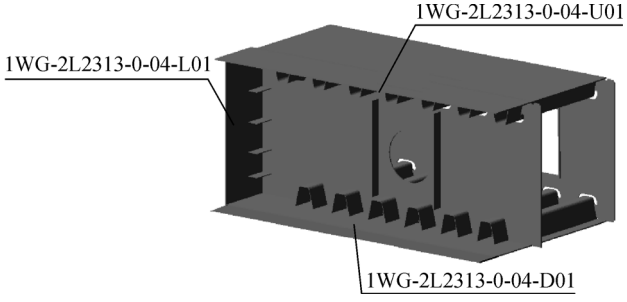

Fig. 13 BIM of the steel box girder

5.2 Benefit evaluation of virtual pre-assembly

5.2.1 Financial aspects

(1) Cost of equipment and modeling

This project is mainly for the splicing of steel box girders. The quotation of light pen measurement is presented as follows. The BIM cost mainly includes software, computer, modeling, development, and other costs (Zhao and Yuan, 2015). Table 2 is based on market conditions and actual costs.

In summary, the cost of equipment plus modeling is 1254781 CNY.

(2) Operation costs

Operating costs mainly include labor, training, data archiving, and maintenance costs, which are approximately 3 h per week. In the operation process, system maintenance and data collection are required. The use of a pre-assembly method mainly reduces labor, mechanical, and site use costs.

1) Space costs

According to market prices, the leasing price of the factory is generally 1–2.8 CNY·d^{-1}·m^{-2}. According to the regional and regional differences, the price in Wuhan is approximately 1.4 CNY·d^{-1}·m^{-2}. The traditional field pre-assembly takes nearly 15 d in accordance with the average length and width of the bridge length and segment (13 m×4.5 m), which are available at a site cost of $1.4\times15\times13\times4.5\times1826=2243241$ CNY.

2) Labor costs

Following the information price of Wuhan City in 2016, the median wage is taken, and the average salary of heavy, electric welders, and general workers is considered. The average wage is $(118+150.38+128.65)/3=132.34$ CNY·d^{-1}, and all segments are completed. The pre-assembly work takes 1080 d, and the saved available labor cost is 142900 CNY.

In summary, the return on investment using virtual pre-assembly technology can be described as $R=1254781/(2243241+142900)=52.59\%$.

5.2.2 Product aspects

(1) Construction schedule

As shown in the Fig. 14, the pre-splicing on the assembly jigs in the traditional process of this project takes 15 d. The production, hoisting, and demolition times for assembly jigs are 2.5, 0.5, and 3 d, respectively. The on-site measurement during the new process takes 21 d. A total of 7.5 d are spent on modeling and assembling.

The shortened section production period indicates that the total time difference between subsequent processes (segment transportation, hoisting, and welding) will be long, and the relevant measures for taking off work will be decreased. Meanwhile, the completion of the project in advance will leave an excellent impression on Party *A* and obtain relevant early completion reward.

(2) Quality

Before and after the application of virtual pre-assembly technology, the qualification rate of manufactured steel structural parts is 100%.

5.2.3 Organizational aspects

The survey indicates that, after the project has applied the

Table 2 Virtual pre-assembly costs

Aspects	Details	Uses	Quantity	Unit price/CNY	Total/CNY
Software	Revit/Navisworks	Modeling/presentation	1		Addition to consultation cost
Hardware	Computers	Saving/presentation	4	10000	40000
Consultation cost	BIM technology	Modeling/system developing/detection/ software copyright/training	1	500000	500000
3D measurement	Measuring equipment/service	Equipment/service/training/transport costs	1	714781	714781

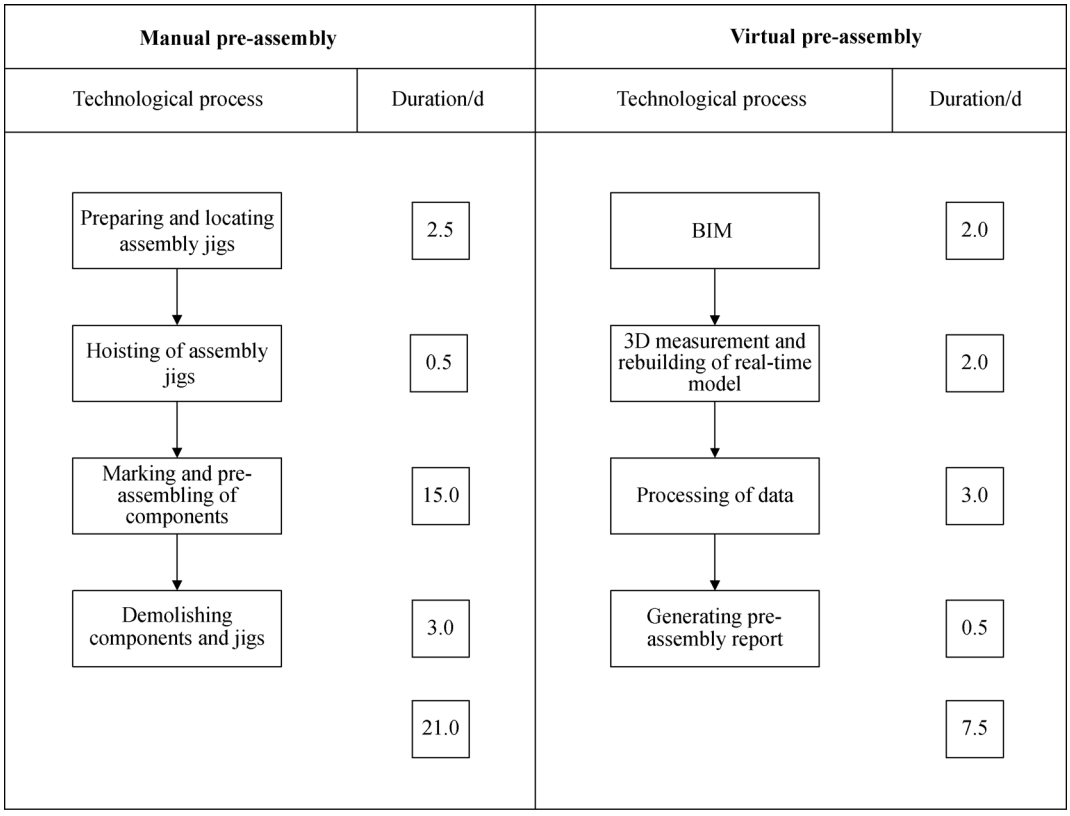

Fig. 14 Duration comparison between manual and virtual pre-assembly

offline assembly technology, the project management personnel has a certain understanding of the offline assembly technology and can apply this technology to the next project.

5.2.4 Management aspects

(1) Communication

During manufacturing of steel structures, the process of saving the splicing section on the assembly jigs and the information request of the engineering assembling instruction in the pre-splicing process are decreased.

(2) Production efficiency

The traditional process requires no rework. Conversely, some components are reworked during the process of using offline technology to control the error of steel components. The number of statistical welding corrections for plate units in 1826 segments is approximately 40, and the rate of rework increase is 2.19%.

5.2.5 Future development

(1) Competitive superiority

The virtual pre-assembly method of steel structural parts can be used not only for the manufacture of beams for bridge construction but also for the quality inspection of steel structures in construction and municipal engineering, especially for the control of errors in steel structures of super high-rise buildings, effective storage of data, and improvement in data utilization.

(2) Customer satisfaction

The project is completed on time, thereby reaching the requirements of the owners and meeting the delivery requirements.

6 Conclusions and discussion

This study proposes a virtual assembly method for steel structures based on BIM technology, PLP algorithm, and 3D measurement. In this method, 3D measurement, coordinate alignment, model correction, and virtual assembly are all performed in the same processor to avoid convergence between two programs. This method is applied to practical projects, and its benefits are evaluated. Under the ideal condition of applying this method, the new technology reduces the flow of assembling and dismantling of components on the assembly jigs and saves operating costs such as space rental (including mechanical use) and welding labor. The proposed method provides a new idea for the pre-assembly work of structures.

The proposed method can be a reference for future pre-assembly work. However, the suitability of this method to

other types of project is not discussed. Projects with relatively small number of component units may still suitably use traditional pre-assembly technology. Therefore, the scale of the project should be considered when using the proposed method.

Acknowledgements The presented work has been supported by the National Natural Science Foundation of China (NSFC) through grant 71471072 and Hubei Technical Innovation Project through grant 2017ACA186.

References

Azhar S, Nadeem A, Mok J Y N, Leung B H Y (2008a). Building information modeling (BIM): a new paradigm for visual interactive modeling and simulation for construction projects. In: Proceedings of the First International Conference on Construction in Developing Countries (ICCIDC-I), Karachi, Pakistan

Azhar S, Hein M, Sketo B (2008b). Building information modeling (BIM): benefits, risks and challenges. In: Proceedings of the 44th Annual Conference of the Associated Schools of Construction, Auburn, USA, 1–11

Barone S, Paoli A, Razionale A V (2012). Shape measurement by a multi-view methodology based on the remote tracking of a 3D optical scanner. Optics and Lasers in Engineering, 50(3): 380–390

Bjorhovde R (2012). Concepts and implementation of strain-based criteria in design codes for steel structures. Frontiers of Structural and Civil Engineering, 6(3): 210–216

Case F, Beinat A, Crosilla F, Alba I M (2014). Virtual trial assembly of a complex steel structure by generalized Procrustes analysis techniques. Automation in Construction, 37(1): 155–165

Chen W, Zeng W, Tong M, Yan J (2015). Comparative analysis of the solid waste emissions between the industrialized and traditional residential building. Frontiers of Engineering Management, 2(2): 188–192

Chen Z H, Du F Z, Tang X Q (2013). Research on uncertainty in measurement assisted alignment in aircraft assembly. Chinese Journal of Aeronautics, 26(6): 1568–1576

Crispin A J, Rankov V (2007). Automated inspection of PCB components using a genetic algorithm template-matching approach. International Journal of Advanced Manufacturing Technology, 35(3–4): 293–300

Ding Y, Lu H, Li W (2012). The application of information technology pre-assembly in finished product inspection & test of steel structures. Journal of Information Technology in Civil Engineering & Architecture, 4(1): 52–56 (in Chinese)

Fan S L, Kang S C, Hsieh S H, Chen Y H, Wu C H, Juang J R, (2009). A case study on constructing 3D/4D BIM models from 2D drawings and paper-based documents using a school building project. In: Proceedings of International Conference Computational Design in Engineering, Seoul, Korea, 77–94

Han Y, Wu Y B, Cao D H, Yun P (2017). Defect detection on button surfaces with the weighted least-squares model. Frontiers of Optoelectronics, 10(2): 151–159

Hara K, Shimbo M, Okuma H (2009). Coordinate structure analysis with global structural constraints and alignment-based local features. In: Proceedings of the 47th Annual Meeting of the Association for Computational Linguistics and the 4th International Joint Conference on Natural Language Processing of the AFNLP, Suntec, France, 967–975

Jayaram S, Connacher H I, Lyons K W (1997). Virtual assembly using virtual reality techniques. Computer Aided Design, 29(8): 575–584

Lan M, Wang Y, Feng J (2013). Application of preassembly technology of steel structure simulated by computer. Industrial Construction, 43(S1): 713, 722–723 (in Chinese)

Leão R J, Baldo C R, Reis M L C C, Trabanco J L A, Rodrigues F, Neuenschwander R T (2017). Magnet alignment on a common girder: development of a length artefact for measurement accuracy improvement. Precision Engineering, 50: 53–62

Li W B, Lu C H, Zhang J C (2013). A lower envelope weber contrast detection algorithm for steel bar surface pit defects. Optics & Laser Technology, 45(1): 654–659

Li Y, Yao J, Zhang Y (2016). Theoretical research on virtual trial assembly. Industrial Construction, 46(1): 147–154 (in Chinese)

Li Y, Zhang L, Wang Y (2017). An optimal method of posture adjustment in aircraft fuselage joining assembly with engineering constraints. Chinese Journal of Aeronautics, 30(6): 2016–2023

Liu P, Wei Y, Qiu Y P (2007). New technology for design of modern aircraft assembly jig. Hongdu Science & Technology, 2007(3): 17–21 (in Chinese)

Liu X, Xie N, Tang K, Jia J (2016). Lightweighting for Web3D visualization of large-scale BIM scenes in real-time. Graphical Models, 88: 40–56

Lu N, Korman T (2010). Implementation of building information modeling (BIM) in modular construction: benefits and challenges. In: Proceedings of Construction Research Congress 2010, Banff, Canada, 1136–1145

MacWilliams B A, Desjardins J D, Wilson D R, Romero J, Chao E Y S (1998). A repeatable alignment method and local coordinate description for knee joint testing and kinematic measurement. Journal of Biomechanics, 31(10): 947–950

Meng X P (2017). Research on coordinate alignment method of portable coordinate measuring instrument. Technology Innovation and Application, 2017(27): 64–65 (in Chinese)

Paoli A, Razionale A V (2012). Large yacht hull measurement by integrating optical scanning with mechanical tracking-based methodologies. Robotics and Computer-integrated Manufacturing, 28(5): 592–601

Radowick D G (2003). US Patent, 6546616, 2003-4-15

Smith D K (2007). Building Information Modeling: A Strategic Implementation Guide for Architects, Engineers, Constructors, and Real Estate Asset Managers. Hoboken: John Wiley & Sons, Inc., 12–14

Spence J W, Lipfert F W, Katz S (1993). The effect of specimen size, shape, and orientation on dry deposition to galvanized steel surfaces. Atmospheric Environment, 27(15): 2327–2336

Sun H M, Yao L B (2008). Transformation between alignment coordinates and engineering coordinates and its application. Surveying & Mapping of Geology and Mineral Resources, 24(3): 15–17 (in Chinese)

Tamai S, Yagata Y, Hosoya T (2002). New technologies in fabrication of

steel bridges in Japan. Journal of Constructional Steel Research, 58(1): 151–192

Tang J Y, Wu L N, Liao G H (2009). Application of simulation assembly technology for steel structure in Kunming new airport terminal. Construction Technology, 2009(12): 21–24 (in Chinese)

Wang B R, Guo F Y, Xiao J, Zeng C, Zhou X (2016). Research on digital simulation pre-assembly technology of steel structure based on high precision laser total station. Architecture Construction, 38(12): 1726–1729 (in Chinese)

Zhao B, Yuan S (2015). Research on the BIM application modes and benefit evaluation based on the owners drive. Construction Economy, 36(4): 15–19 (in Chinese)